Recent intensification of wind-driven circulation in the Pacific and the ongoing warming hiatus

Matthew H. England[1,2]*, Shayne McGregor[1,2], Paul Spence[1,2], Gerald A. Meehl[3], Axel Timmermann[4], Wenju Cai[5], Alex Sen Gupta[1,2], Michael J. McPhaden[6], Ariaan Purich[5] and Agus Santoso[1,2]

Despite ongoing increases in atmospheric greenhouse gases, the Earth's global average surface air temperature has remained more or less steady since 2001. A variety of mechanisms have been proposed to account for this slowdown in surface warming. A key component of the global hiatus that has been identified is cool eastern Pacific sea surface temperature, but it is unclear how the ocean has remained relatively cool there in spite of ongoing increases in radiative forcing. Here we show that a pronounced strengthening in Pacific trade winds over the past two decades—unprecedented in observations/reanalysis data and not captured by climate models—is sufficient to account for the cooling of the tropical Pacific and a substantial slowdown in surface warming through increased subsurface ocean heat uptake. The extra uptake has come about through increased subduction in the Pacific shallow overturning cells, enhancing heat convergence in the equatorial thermocline. At the same time, the accelerated trade winds have increased equatorial upwelling in the central and eastern Pacific, lowering sea surface temperature there, which drives further cooling in other regions. The net effect of these anomalous winds is a cooling in the 2012 global average surface air temperature of 0.1–0.2 °C, which can account for much of the hiatus in surface warming observed since 2001. This hiatus could persist for much of the present decade if the trade wind trends continue, however rapid warming is expected to resume once the anomalous wind trends abate.

Observations of global average surface air temperature (SAT) show an unequivocal warming over the twentieth century[1], however the overall trend has been interrupted by periods of weak warming or even cooling (Fig. 1). For example, warming largely stalled from the 1940s to the 1970s. Between 1975 and 2000 the overall upward SAT trend resumed, but it was not uniform, with a decade of accelerated warming from about 1975–1985 (ref. 2), as well as periods of little warming[3]. Since around 2001 a marked hiatus in global surface warming has occurred, raising questions about its cause, its likely duration and the implications for global climate change.

Decadal periods of minimal warming, or even cooling, interspersing decades of rapid warming, are not inconsistent with a long-term warming trend; indeed this characterizes the interplay between steadily increasing greenhouse gas forcing and internally generated climate variability. Factors other than internal variability, such as volcanoes and changes in solar radiation, can also drive cooler decades against the backdrop of ongoing warming. Indeed, hiatus decades are expected to punctuate future warming trends, even under scenarios of rapid global warming[4,5]. Mechanisms proposed to explain the most recent observed hiatus include increased ocean heat uptake[2,3,6,7], the prolonged solar minimum[4] and changes in atmospheric water vapour[8] and aerosols[9,10]. The cool surface waters of the eastern Pacific have also been linked to the global temperature hiatus[11] and consensus is building that the subsurface ocean, with its vast capacity for heat storage, is playing a significant role through enhanced heat uptake[2,3,7,12,13]. It remains unclear, however, where the bulk of anomalous ocean heat uptake

has occurred, with the Pacific[2,3], Atlantic[13,14] and Southern[14–17] Oceans all potential candidates.

One notable aspect of the two most recent extended hiatus periods (1940–1975 and 2001–present), in contrast to periods of global SAT warming (1910–1940 and 1976–2000), is that they correspond closely to periods when the Interdecadal Pacific Oscillation[18–20] (IPO) has been in a negative phase (Fig. 1a). The IPO manifests as a low-frequency El Niño-like pattern of climate variability, with a warm tropical Pacific and weakened trade winds during its positive phase, and a cool tropical Pacific and strengthened winds during its negative phase. Recent analyses of climate model simulations suggest that hiatus decades are linked to negative phases of the IPO (refs 2,3,11). Here we examine the most recent hiatus in this context, particularly in relation to altered ocean dynamics and enhanced ocean heat uptake, and assess implications for the coming decades.

To examine the ongoing hiatus compared with a period of warming, we start by considering climatic trends over the past two decades, spanning the transition from a period of global surface warming in the 1990s to the post-2000 hiatus. During this time the Pacific trade winds increased substantially[21] (Figs 1b and 2a), including both the Walker and Hadley circulation components, as reflected in anomalously high sea level pressure (SLP) centred at mid-latitudes (Fig. 2a). This trend in SLP and wind stress is consistent with the change in sign of the IPO in the late 1990s (ref. 22 and Fig. 1b), although the wind trends are even stronger and larger scale than those typically associated with the IPO, with the IPO regressed winds accounting for only approximately half the

[1]ARC Centre of Excellence for Climate System Science, University of New South Wales, New South Wales 2052, Australia, [2]Climate Change Research Centre, University of New South Wales, New South Wales 2052, Australia, [3]National Center for Atmospheric Research, Boulder, Colorado 80307, USA, [4]International Pacific Research Centre, University of Hawaii, Hawaii 96822, USA, [5]CSIRO Marine and Atmospheric Research, Aspendale, Victoria 3195, Australia, [6]NOAA/Pacific Marine Environmental Laboratory, Seattle, Washington 98115, USA. *e-mail: m.england@unsw.edu.au
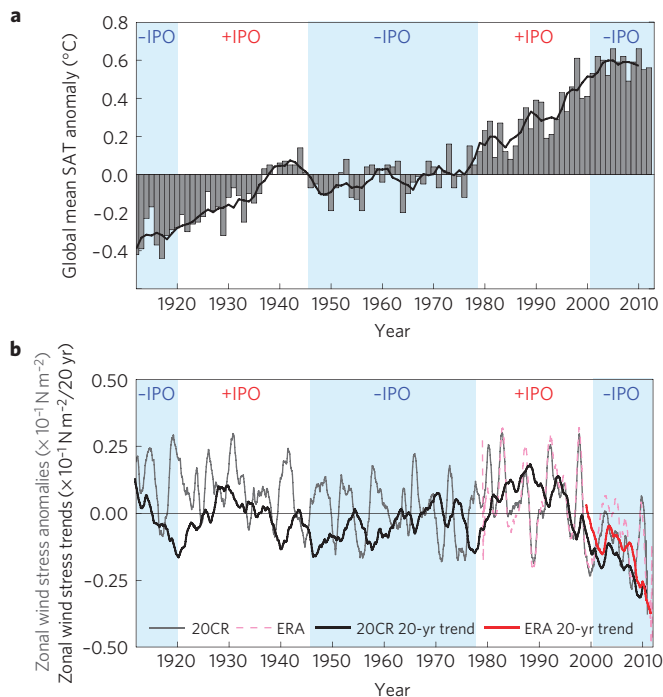
Figure 1 | Global average SAT and Pacific trade wind anomalies over the past century. a, Temperature anomalies are shown as the annual mean relative to 1951–1980, with individual years shown as grey bars and a five-year running mean overlaid in bold. **b**, Pacific wind stress anomalies are computed over the region 6° N–6° S and 180°–150° W (green rectangle in Fig. 2a), corresponding to where the IPO exhibits maximum regression onto Pacific Ocean winds. Anomalies are shown relative to the historical record for two climatologies (Methods), with a bold line indicating the strength of the 20-year trends leading up to each year shown. In both reanalysis products shown, the recent multidecade acceleration in Pacific trade winds is the highest on record, although estimates of observed winds are not well constrained by measurements previous to the satellite era. The sign of the low-pass filtered IPO index[18,19] is indicated in both panels, with negative phases of the IPO shaded in blue.

magnitude of the observed change (Supplementary Fig. 1). The wind trend is thus probably due to both the recent change in the IPO (associated with a change in ENSO statistics[23] and forced by internal variability, and/or external forcing such as volcanic emissions, solar irradiance and aerosols), along with other factors, such as recent rapid warming in the Indian Ocean[24,25].

The impact of the acceleration in Pacific winds is apparent in sea level trends[26,27] (Fig. 2b) and changes in ocean circulation (Supplementary Fig. 2). Although measurements are generally too sparse to constrain observed trends in ocean circulation, estimates derived from reanalysis products suggest an acceleration of the equatorial jets and an increase in wind-driven Ekman divergence away from the Equator over the past two decades (Supplementary Fig. 2). In the central and western Pacific there is evidence for increased equatorial pycnocline convergence of mass and heat, and an associated acceleration of the equatorial undercurrent (Fig. 3 and Supplementary Fig. 2). The enhanced convergence in the tropical pycnocline drives a net heat gain in the ocean interior, while the increased upwelling generates a cooling at the surface in the east Pacific (Fig. 3).

Sea surface temperature (SST) has thus also changed in the Pacific, with the pattern of change matching that expected from an acceleration of the trade winds, an increase in equatorial upwelling and a spin-up of the subtropical gyres (Fig. 2c). This includes
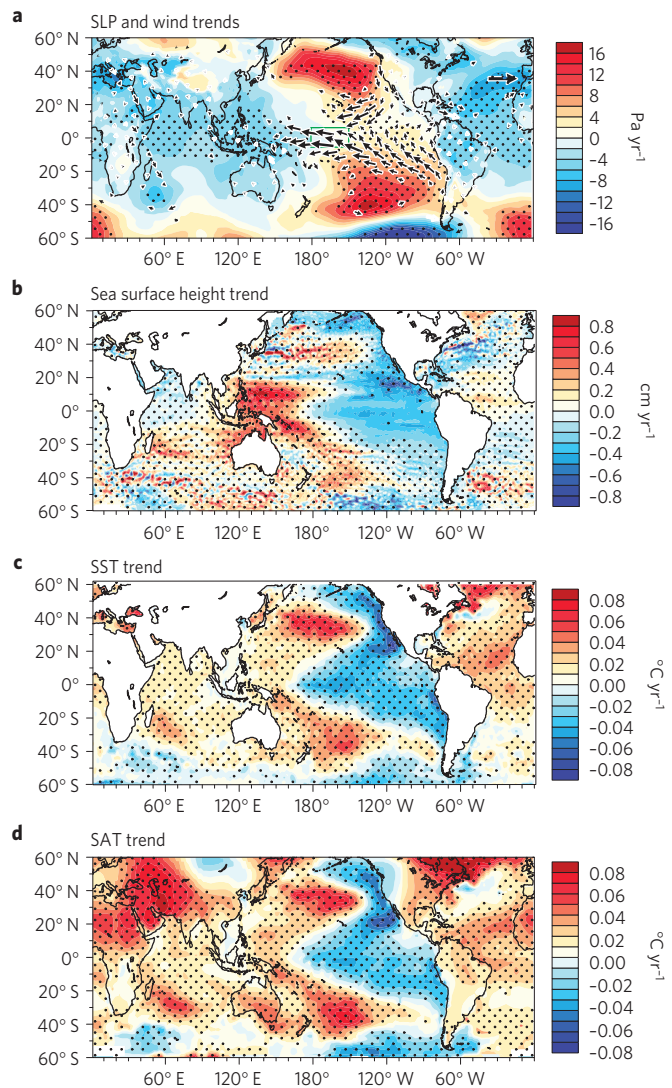
Figure 2 | Observed trends in winds, SLP, sea surface height, SST and SAT during 1992–2011. a, Observed trends in surface wind stress (N m^{-2} yr^{-1}) shown as vectors with observed trends in atmospheric SLP overlaid in colour shading (Pa yr^{-1}). The maximum vector is 0.003 N m^{-2} yr^{-1} and only vector trends that are significant at the 95% confidence level are shown. The green rectangle is the region computed in Fig. 1b. **b**, Observed trends in sea surface height (cm yr^{-1}) from satellite altimetry. **c,d**, Observed trends in SST (**c**) and surface layer air temperature (**d**), respectively (°C yr^{-1}). In all panels, stippling indicates where the trends are significant at the 95% confidence level given the linear regression standard error over the entire period of 1992–2011.

warming in the Western Pacific Warm Pool, warming in the western boundary[28] and cooling over the tropical central and eastern Pacific. The east Pacific cooling extends polewards along the coast of the Americas, consistent with an acceleration of the North and South Equatorial Currents, and the North Pacific subtropical gyre. SAT trends (Fig. 2d and Supplementary Fig. 3) largely reflect the trends seen in SST.

To quantify the impact of recent trends in Pacific winds on climate, we first examine a global ocean model subject to historical changes in radiative forcing coupled to a simple energy–moisture balance atmosphere forced by prescribed winds (Methods). This enables an examination of the oceanic response to the observed Pacific wind trends without atmospheric feedbacks. In parallel
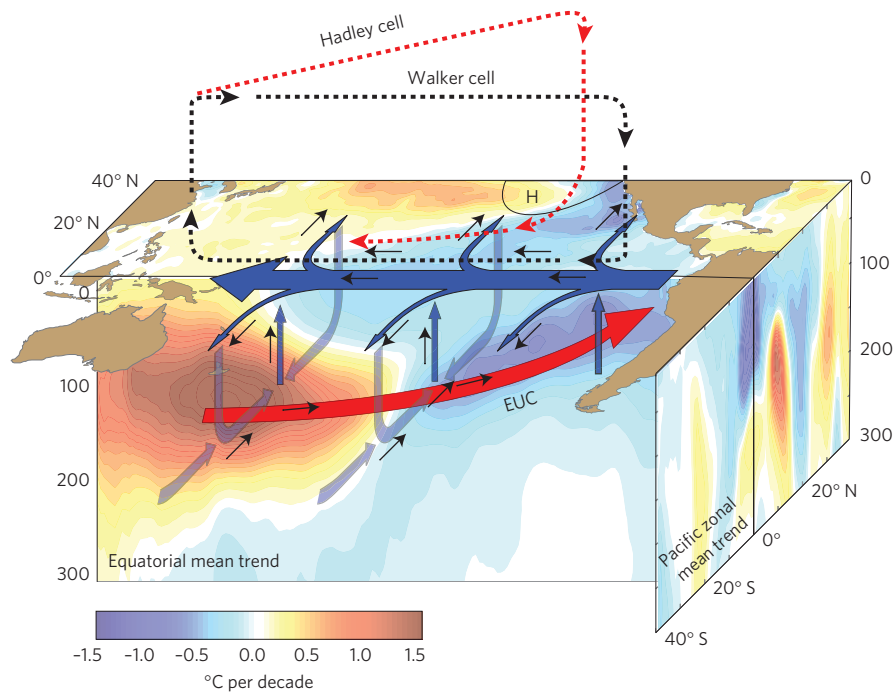
Figure 3 | Schematic of the trends in temperature and ocean–atmosphere circulation in the Pacific over the past two decades. Colour shading shows observed temperature trends (°C per decade) during 1992–2011 at the sea surface (Northern Hemisphere only), zonally averaged in the latitude-depth sense (as per Supplementary Fig. 6) and along the equatorial Pacific in the longitude-depth plane (averaged between 5° N–5° S). Peak warming in the western Pacific thermocline is 2.0 °C per decade in the reanalysis data and 2.2 °C per decade in the model. The mean and anomalous circulation in the Pacific Ocean is shown by bold and thin arrows, respectively, indicating an overall acceleration of the Pacific Ocean shallow overturning cells, the equatorial surface currents and the Equatorial Undercurrent (EUC). The accelerated atmospheric circulation in the Pacific is indicated by the dashed arrows; including the Walker cell (black dashed) and the Hadley cell (red dashed; Northern Hemisphere only). Anomalously high SLP in the North Pacific is indicated by the symbol 'H'. An equivalent accelerated Hadley cell in the Southern Hemisphere is omitted for clarity.

experiments, we later re-evaluate the impact of the Pacific winds in a full coupled climate model setting. Two types of experiment are undertaken in each model setting: one forced by climatological monthly varying winds, the other includes the addition of observed 1992–2011 Pacific wind trend anomalies (Fig. 2a and Methods).

The ocean model SST response to the applied wind trends captures the pattern of recent warming and cooling observed over the Pacific Ocean (compare Figs 4a and 2c), with cooling in the central and east and warming in the west that extends into the Indian Ocean and polewards in the tropical Pacific western boundaries. Peak cooling in the central Pacific is higher than observed, although elsewhere the pattern and magnitude agree well. Ocean velocity and horizontal streamfunction trends (Fig. 4a and Supplementary Figs 4 and 5) demonstrate that the simulation reproduces many of the changes seen in the reanalysis data; for example, an acceleration in surface Ekman divergence and pycnocline convergence, a spin-down in the tropical Pacific western boundary currents and an increase in both the Indonesian throughflow and the Equatorial Undercurrent. The Kuroshio Current and the North Pacific gyre also accelerate.

Subsurface temperature and circulation fields also exhibit significant trends, with a cooling in the upper tropical ocean and warming at depth, consistent with observational evidence (Fig. 3 and Supplementary Fig. 6). The maximum rate of warming in the tropical Pacific thermocline agrees well between model (2.2 °C per decade) and reanalysis data (2.0 °C per decade). The circulation trends reveal an acceleration of the Pacific Ocean shallow overturning cells[22] (Fig. 4b), as identified during hiatus periods in the National Center for Atmospheric Research (NCAR) climate model[2,3], driven by an intensified wind stress curl on either side of the Equator. The enhanced overturning cells increase

both the upwelling of cool subthermocline waters at the Equator and the subduction of warm subtropical water into the ventilated thermocline (Supplementary Figs 4 and 6), enhancing convergence in the tropical pycnocline (Fig. 3 and Supplementary Fig. 4). This increases the subsurface uptake of heat in the Pacific, while cooling the surface layer that interacts with the atmosphere. Differences in heat content in 2012 between the two experiments confirm this, with a net wind-driven heat gain below 125 m ($+5.0 \times 10^{22}$ J; most of this in the Pacific and Indian Oceans) and reduced heat content in the surface 125 m (-3.8×10^{22} J), resulting in a net ocean heat gain of 1.2×10^{22} J. This is about half the model's total integrated radiation imbalance at the top of the atmosphere during the post-2000 hiatus, reducing SAT trends during this decade.

The Pacific wind trends thus produce a cooler tropical Pacific and other ocean circulation changes that contribute to a cooler global average SAT, although the influence on global average temperatures becomes detectable only ∼5 years after the start of the trade wind acceleration (Fig. 4c). This spin-up in heat uptake in the subtropical overturning cells matches the approximate timescale for baroclinic wave adjustment to changing wind stress at subtropical latitudes[22]. Furthermore, about 80% of the cooling in SAT occurs post-2000, suggesting that the multidecadal Pacific wind acceleration is an integral element to account for the hiatus of the scale recently observed (this is also the case in models; Supplementary Fig. 7). Relative to the control greenhouse warming experiment, anomalous global average SAT cooling due to Pacific wind trends reaches ∼0.11 °C by 2012 (Fig. 4c), consistent with the extra heat stored by the ocean.

Projections of global surface warming estimated from the two most recent generations of coupled climate models assessed by the Intergovernmental Panel on Climate Change (IPCC; Methods)
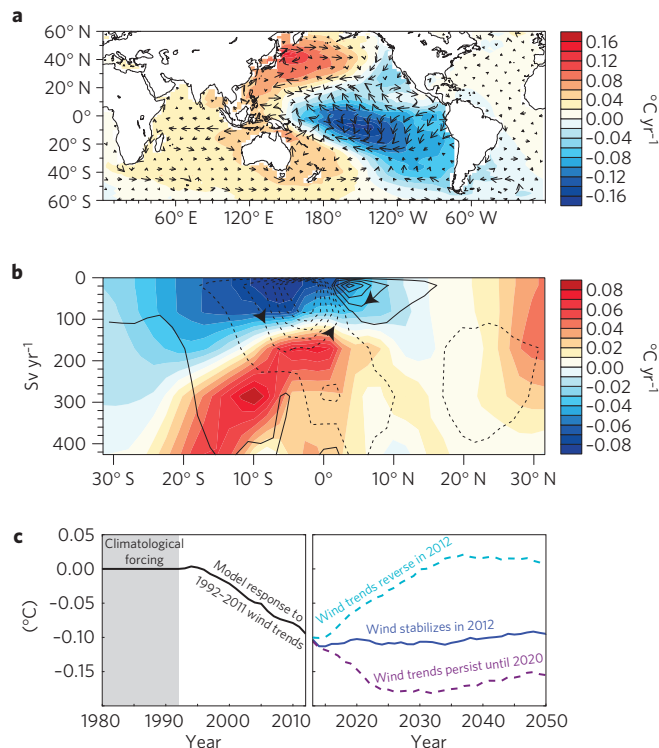
Figure 4 | Model temperature and ocean circulation anomalies due to observed 1992–2011 wind trends over the Pacific Ocean, and projections to 2050. a, SST and ocean circulation trends in the model experiment including both historical CO_2 forcing and observed 1992–2011 Pacific Ocean wind trends. Note the colour scale used is different from the observed trends (Fig. 2c). **b**, As in **a** but showing the zonal average temperature and meridional overturning circulation trends in the Pacific Ocean. Units are °C yr^{-1} and Sv yr^{-1}, respectively. Maximum vector in **a** is 1 cm s^{-1} per 20 yr (trends larger than this are shown on this maximum scale, for clarity). Contour interval is 0.2 Sv yr^{-1} in **b** with contours drawn at ±0.1, ±0.3, ±0.5, ±0.7,… Sv yr^{-1}. Solid (dashed) contours indicate a clockwise (anticlockwise) circulation. **c**, Wind-induced annual mean global SAT anomalies relative to the increasing CO_2 experiment during 1980–2012 and projected for 2013–2050 assuming (i) a return to climatological winds by 2030, (ii) a fixed wind anomaly from 2012 onwards and (iii) a continuation of the recent trend until 2020 and stabilization thereafter. Future SAT anomalies essentially track the wind trend after 2013: either returning to zero by 2030, persisting at around 0.1 °C cooling or increasing up to 0.18 °C cooling by 2025.

generally overshoot the observed global mean SAT during the last few years of the recent hiatus[29] (Fig. 5a) unless the models are initialized by observations[30]. However, after adjusting these projections by adding the anomalous cooling induced by the 1992–2011 Pacific wind trends, the observations lie within the multi-model range (Fig. 5a, blue envelope). Furthermore, the wind-induced cooling can account for approximately 50% of the observed hiatus when comparing the observed and model SAT projections to 2012 (Fig. 5a). Much of the rest of the hiatus can be accounted for when the wind trends are further prescribed in a fully coupled ocean–atmosphere model (Methods; Fig. 5a, green curve). This results from remote atmospheric teleconnections driven by the east Pacific cooling (Supplementary Fig. 8), consistent with a recent study applying specified east Pacific SST to model the global hiatus[11].

The addition of these wind-induced cooling anomalies to multi-model mean projections (Fig. 5a) is justified as multidecadal wind variability is neither synchronous across models nor with observations. As such, the impact of any internally generated

wind variability is largely cancelled out in the multi-model mean. Furthermore, none of 48 climate model experiments examined in detail captures the magnitude of the recent acceleration in Pacific trade winds (Supplementary Fig. 9). In fact the most extreme acceleration seen in the models is generally less than half that observed (see also Fig. 5b). The wind-adjusted envelopes in Fig. 5a can thus be thought of as the approximate projection range had all models captured the recent 20-year trend in Pacific winds. Adding this wind-induced cooling leaves the observed hiatus within the range of recent model projections.

The envelope of adjusted climate projections beyond 2013 is also significantly impacted by the Pacific wind trends; in the coupled system this depends critically on how tropical wind patterns evolve over the next decade (Fig. 5a). In the scenario where the trade wind trends persist further, the coupled model remains in a hiatus to almost 2020 (Fig. 5a; black dashed curve), with global average air temperatures not warming significantly above the 2001–2010 mean, reminiscent of the extended 1940–1975 hiatus (Fig. 1a and Supplementary Fig. 10). In contrast, if the anomalously strong trade winds begin to abate in the next few years, the model suggests the present hiatus will be short-lived (Fig. 5a, green curve), with rapid warming set to resume soon after the wind trends reverse.

Methods

Observations and reanalysis data. SAT is taken from the Goddard Institute for Space Studies (GISS) climatology[31,32]. Recent observed winds and SLP are taken from the interim European Centre for Medium-Range Weather Forecasts (ECMWF) Re-Analysis (ERA-Interim[33]). Winds from earlier in the twentieth century are from the National Oceanic and Atmospheric Administration (NOAA) reanalysis[34]. The 1992–2011 trade wind trend is robust across various climatologies[26]. Sea surface height is taken from the Archiving, Validation, and Interpretation of Satellite Oceanographic (AVISO) data set. SST is from the Hadley Centre climatology[35]. Various reanalysis products[36–40] are used to assess recent interior ocean temperature and circulation trends. The IPO index (Fig. 1) is calculated as per ref. 19.

Wind-forced ocean model experiments. A fully dynamic ocean circulation model coupled to an atmospheric energy–moisture balance model[41] is used to assess the impact of wind trends on ocean heat uptake, in isolation of atmospheric circulation feedbacks. The ocean component is purposefully configured to match the resolution and parameters of typical models used in the Coupled Model Intercomparison Project Phase 5 (CMIP5). Atmospheric heat and moisture are fully coupled to the other model components, whereas wind fields are prescribed, which has the advantage of allowing us to quantify the impact of Pacific wind trends on ocean heat uptake and cooling of the atmosphere, in isolation of other feedbacks. As such, for this model, single runs are sufficient and no multi-experiment ensemble analysis is required.

After the model is equilibrated with atmospheric CO_2 fixed at pre-industrial, a control experiment is integrated from 1900 to 2012 forced by historical reconstructed greenhouse gas concentrations and other natural and anthropogenic factors, including anthropogenic aerosols (volcanic aerosols are not included). The model's depth-integrated ocean heat content change in the upper 2000 m from 1990 to 2012 (19×10^{22} J; equivalent to 0.51 W m^{-2}) compares well to observed estimates[14] ($\sim 16 \times 10^{22}$ J or 0.43 W m^{-2}, noting this estimate is considered conservative[42]). This suggests that the overturning circulation and large-scale mixing of heat into the interior is well reproduced by the model. The model is also able to capture the overall twentieth-century SAT trend, giving confidence that it resolves the broad-scale cycling of heat between the atmosphere, ocean, ice and land surface systems.

The Pacific wind perturbation experiments replicate the control, but there is a linear wind anomaly trend applied between 45° N and 45° S (smoothed to zero between 40–45° N and 40–45° S), beginning in 1992 and reaching a maximum at the end of 2011, based on the observed linear best fit trends in the ERA-Interim monthly wind stress climatology[33] during 1992–2011 (as depicted in Fig. 2a). Wind speed trends during this time are also applied to the ocean–atmosphere latent and sensible heat fluxes. The direct wind stress impacts are found to dominate the forcing response, however, with wind-altered buoyancy fluxes secondary.

Beyond 2012, the experiments are integrated following the Representative Concentration Pathway (RCP) 6 emission scenario[43]. In addition, three different future Pacific wind trend scenarios are run from 2012 to 2100, wherein (1) there is a linear ramp-down of the Pacific Ocean winds back to climatological values by
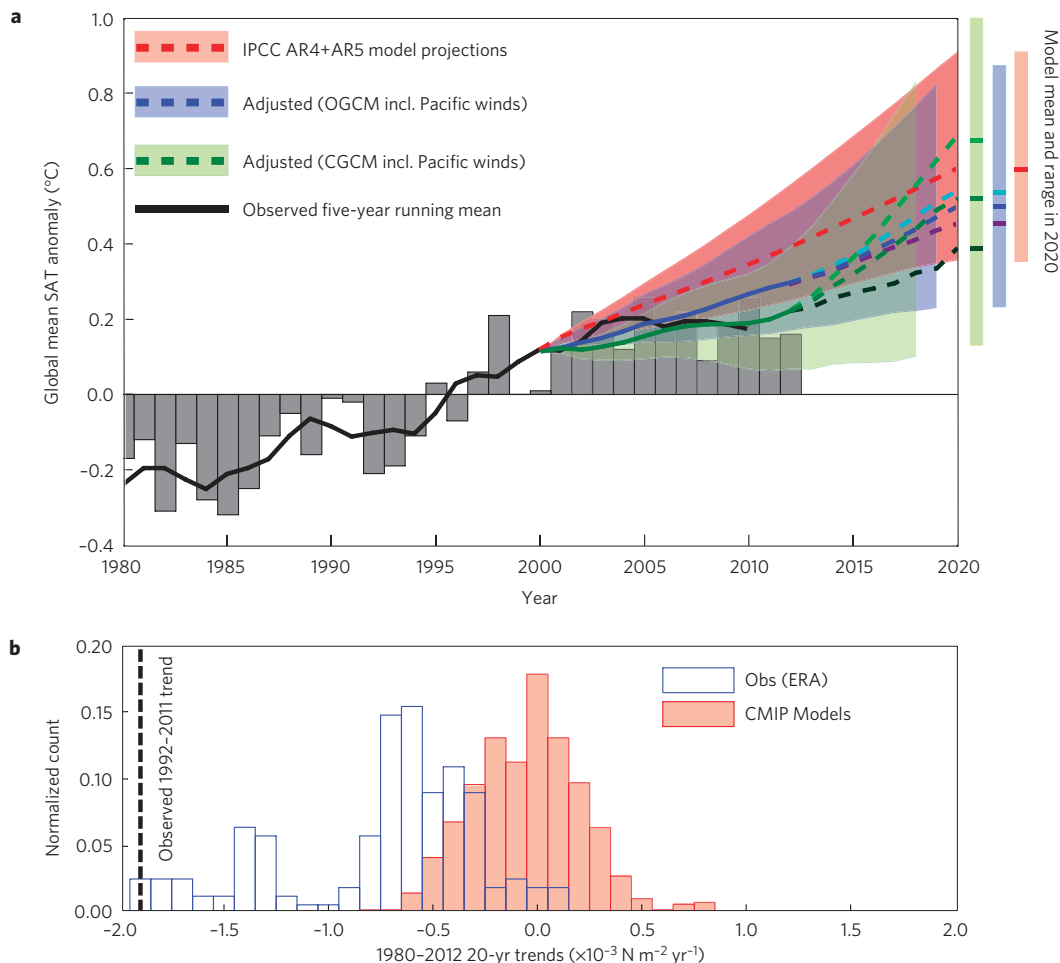
Figure 5 | Recent annual average global air temperature anomalies and Pacific wind trends compared with model projections. a, Observations are shown as annual anomalies relative to the 1980–2012 mean (grey bars) and a five-year running mean (black solid line). Model projections are shown relative to the year 2000 and combine the CMIP3 and CMIP5 multi-model mean (red dashed line) and range (red shaded envelope). The projections branch off the five-year running mean of observed anomalies and include all simulations as evaluated by the IPCC AR4 and AR5. The cyan, blue and purple dashed lines and the blue shading indicate projections adjusted by the trade-wind-induced SAT cooling estimated by the ocean model (OGCM), under three scenarios: the recent trend extends until 2020 before stabilizing (purple dashed line); the trend stabilizes in year 2012 (blue dashed line); and the wind trend reverses in 2012 and returns to climatological mean values by 2030 (cyan dashed line). The black, dark green and light green dashed lines are as per the above three scenarios, respectively, only using the trade-wind-induced SAT cooling derived from the full coupled model (CGCM). Shading denotes the multi-model range throughout. **b**, Normalized histograms of Pacific trade wind trends (computed over 6° N–6° S and 180°–150° W) for all 20-year periods using monthly data in observations (1980–2011) versus available CMIP5 models (1980–2013). The observed trend strength during 1992–2011 is indicated.

2030, (2) the wind anomalies remain constant from 2012 onwards, and lastly (3) the imposed upward wind trend is continued until 2020, before stabilizing and then remaining constant until the end of the model run.

Wind-forced coupled climate model experiments. A full coupled climate model[44,45] is used to further assess the role of the recent observed Pacific wind trends on the ongoing warming hiatus. The model resolves the interactions between the atmosphere, ocean, land and sea-ice components; although during the wind-forced phase, the ocean component instead 'feels' prescribed winds in the Pacific between 45° N–45° S, in all other ways the ocean–atmosphere system freely evolves during the model integration. The model is equilibrated for more than 3,000 years with atmospheric CO_2 fixed at pre-industrial and then integrated during 1780–2030 following historical CO_2 forcing (1780–2000) and then the CMIP3 A2 emissions scenario[46] from the year 2000 onwards. The model's overall climate sensitivity is at the low end range of CMIP3 models (reaching 2.1 °C warming by 2090–2099 relative to 1980–1999); however, as our interest is on the cooling impact of the wind-perturbed experiments relative to the control, low climate sensitivity has little bearing on the results. Two sets of 12 ensemble members were generated including full ocean–atmosphere coupling, only with the ocean component forced by: first, seasonally varying climatological model wind stresses (referenced over the period 1980–2012) over the Pacific domain (45° N–45° S); and second, as per the first, only with the additional observed Pacific wind trends applied during 1992–2011. Three future wind trend

scenarios are also explored to 2030, as per the ocean–EBM model. Throughout all experiments, the atmosphere is free to respond to the resulting changes at the sea surface. We also conducted similar experiments with the Pacific winds freely evolving. In those experiments, the SAT cooling is even stronger due to the combined effect of both the prescribed wind trends and the enhanced wind anomalies owing to the Bjerknes feedback (figure not shown).

Mid-twentieth-century hiatus experiment. A final wind anomaly ocean model experiment is assessed over the twentieth century to investigate the role of interdecadal Pacific wind variability in contributing to the 1940–1975 hiatus. In this experiment CO_2 tracks as per the control, but wind anomalies are now derived from a regression of the IPO index[19] onto the ERA-Interim monthly mean wind climatology. Aerosol impacts are purposefully not included in this experiment to isolate the impacts of the mid-twentieth-century IPO evolution separately from the cooling impact of aerosols. As per the 1992–2011 wind trend simulations, these experiments include wind anomalies applied over just the Pacific Ocean (45° S–45° N) and applied to both the air–sea momentum and buoyancy fluxes.

Coupled climate model intercomparison. We also analysed multi-model ensemble global SAT hindcasts and future projections in climate models that participated in CMIP3 and CMIP5 (Fig. 5a and Supplementary Fig. 3). Furthermore, 48 CMIP5 climate model experiments were assessed in terms of

their simulation of Pacific Ocean multidecadal wind trends (Fig. 5b and Supplementary Fig. 9) and how these wind trends relate to decadal global SAT trends (Supplementary Fig. 7). The CMIP5 simulations employ historical anthropogenic and natural forcings until 2005, thereafter the forcing follows RCP4.5 wherever possible; otherwise experiments adopting RCP8.5 are used. As the hiatus decade analysis runs only until 2013 (Supplementary Fig. 7) and the SAT projections to 2020 (Fig. 5a), this choice of scenario is largely arbitrary.

References

1. Trenberth, K. E. *et al. IPCC Climate Change 2007: The Physical Science Basis* (Cambridge Univ. Press, 2007).
2. Meehl, G. A., Hu, A., Arblaster, J. M., Fasullo, J. Y. & Trenberth, K. E. Externally forced and internally generated decadal climate variability associated with the Interdecadal Pacific Oscillation. *J. Clim.* **26,** 7298–7310 (2013).
3. Meehl, G. A., Arblaster, J. M., Fasullo, J. Y., Hu, A. & Trenberth, K. E. Model-based evidence of deep-ocean heat uptake during surface-temperature hiatus periods. *Nature Clim. Change* **1,** 360–364 (2011).
4. Hansen, J., Sato, M., Kharecha, P. & von Schuckmann, K. Earth's energy imbalance and implications. *Atmos. Chem. Phys.* **11,** 13421–13449 (2011).
5. Easterling, D. R. & Wehner, M. F. Is the climate warming or cooling? *Geophys. Res. Lett.* **36,** L08706 (2009).
6. Guemas, V., Doblas-Reyes, F. J., Andreu-Burillo, I. & Asif, M. Retrospective prediction of the global warming slowdown in the past decade. *Nature Clim. Change* **3,** 649–653 (2013).
7. Katsman, C. A. & van Oldenborgh, G. J. Tracing the upper ocean's missing heat. *Geophys. Res. Lett.* **38,** L14610 (2011).
8. Solomon, S. *et al.* Contributions of stratospheric water vapor to decadal changes in the rate of global warming. *Science* **327,** 1219–1223 (2010).
9. Solomon, S. *et al.* The persistently variable 'background' stratospheric aerosol layer and global climate change. *Science* **333,** 866–870 (2011).
10. Kaufmann, R. K., Kauppib, H., Mann, M. L. & Stock, J. H. Reconciling anthropogenic climate change with observed temperature 1998–2008. *Proc. Natl Acad. Sci. USA* **108,** 790–793 (2011).
11. Kosaka, Y. & Xie, S-P. Recent global-warming hiatus tied to equatorial Pacific surface cooling. *Nature* **501,** 403–407 (2013).
12. Watanabe, M. *et al.* Strengthening of ocean heat uptake efficiency associated with the recent climate hiatus. *Geophys. Res. Lett.* **40,** 1–5 (2013).
13. Balmaseda, M. A., Trenberth, K. E. & Källén, E. Distinctive climate signals in reanalysis of global ocean heat content. *Geophys. Res. Lett.* **40,** 1754–1759 (2013).
14. Levitus, S. *et al.* World ocean heat content and thermosteric sea level change (0–2000 m), 1955–2010. *Geophys. Res. Lett.* **39,** L10603 (2012).
15. Lyman, J. M. *et al.* Robust warming of the global upper ocean. *Nature* **465,** 334–337 (2010).
16. Purkey, S. G. & Johnson, G. C. Warming of global abyssal and deep southern ocean waters between the 1990s and 2000s: Contributions to global heat and sea level rise budgets. *J. Clim.* **23,** 6336–6351 (2010).
17. Levitus, S., Antonov, J. & Boyer, T. Warming of the world ocean, 1955–2003. *Geophys. Res. Lett.* **32,** L02604 (2005).
18. Power, S., Casey, T., Folland, C., Colman, A. & Mehta, V. Interdecadal modulation of the impact of ENSO on Australia. *Clim. Dynam.* **15,** 319–324 (1999).
19. Folland, C. K., Renwick, J. A., Salinger, M. J. & Mullan, A. B. Relative influences of the Interdecadal Pacific Oscillation and ENSO on the South Pacific Convergence Zone. *Geophys. Res. Lett.* **29,** 211–214 (2002).
20. Meehl, G. A., Hu, A. & Santer, B. D. The mid-1970s climate shift in the Pacific and the relative roles of forced versus inherent decadal variability. *J. Clim.* **22,** 780–792 (2009).
21. L'Heureux, M. L., Lee, S. & Lyon, B. Recent multidecadal strengthening of the Walker circulation across the tropical Pacific. *Nature Clim. Change* **3,** 571–576 (2013).
22. McPhaden, M. J. & Zhang, D. Pacific Ocean circulation rebounds. *Geophys. Res. Lett.* **31,** L18301 (2004).
23. McPhaden, M. J., Lee, T. & McClurg, D. El Niño and its relationship to changing background conditions in the tropical Pacific Ocean. *Geophys. Res. Lett.* **38,** L15709 (2011).
24. Luo, J. J., Sasaki, W. & Masumoto, Y. Indian Ocean warming modulates Pacific climate change. *Proc. Natl Acad. Sci. USA* **109,** 18701–18706 (2012).
25. Han, W. *et al.* Intensification of decadal and multi-decadal sea level variability in the western tropical Pacific during recent decades. *Clim. Dynam.* (2013) http://dx.doi.org/10.1007/s00382-013-1951-1.
26. McGregor, S., Sen Gupta, A. & England, M. H. Constraining wind stress products with sea surface height observations and implications for Pacific Ocean sea-level trend attribution. *J. Clim.* **25,** 8164–8176 (2012).
27. Merrifield, M. A. A shift in Western Tropical Pacific sea level trends during the 1990s. *J. Clim.* **24,** 4126–4138 (2011).
28. Wu, L. *et al.* Enhanced warming over the global subtropical western boundary currents. *Nature Clim. Change* **2,** 161–166 (2012).
29. Fyfe, J. C., Gillett, N. P. & Zwiers, F. W. Overestimated global warming over the past 20 years. *Nature Clim. Change* **3,** 767–769 (2013).
30. Meehl, G. A. & Teng, H. Case studies for initialized decadal hindcasts and predictions for the Pacific region. *Geophys. Res. Lett.* **39,** L22705 (2012).
31. Hansen, J. *et al.* Global temperature change. *Proc. Natl Acad. Sci. USA* **103,** 14288–14293 (2006).
32. Hansen, J., Ruedy, R., Sato, Mki. & Lo, K. Global surface temperature change. *Rev. Geophys.* **48,** RG4004 (2010).
33. Dee, *et al.* The ERA-Interim reanalysis: Configuration and performance of the data assimilation system. *Q. J. R. Meteorol. Soc.* **137,** 553–597 (2011).
34. Compo, G. P. *et al.* The twentieth century reanalysis project. *Q. J. R. Meteorol. Soc.* **137,** 1–28 (2011).
35. Rayner, N. A. *et al.* Global analyses of sea surface temperature, sea ice, and night marine air temperature since the late nineteenth century. *J. Geophys. Res. (Atmos.)* **108,** 4407 (2003).
36. Carton, J. A., Chepurin, G. A., Cao, X. & Giese, B. A Simple Ocean Data Assimilation retrospective analysis of the global ocean 1950–1995. Part I: Methodology. *J. Phys. Oceanogr.* **30,** 294–309 (2000).
37. Balmaseda, M. A., Mogensen, K. & Weaver, A.T. Evaluation of the ECMWF Ocean Reanalysis System ORAS4. *Q. J. R. Meteorol. Soc.* **139,** 1132–1161 (2013).
38. Mogensen, K., Balmaseda, M. A. & Weaver, A. *The NEMOVAR Ocean Data Assimilation System as Implemented in the ECMWF Ocean Analysis for System 4.* ECMWF Technical Memorandum 668 (2012).
39. Chang, Y-S., Zhang, S., Rosati, A., Delworth, T. L. & Stern, W. F. An assessment of oceanic variability for 1960–2010 from the GFDL ensemble coupled data assimilation. *Clim. Dynam.* **40,** 775–803 (2013).
40. Nishida, T. 2011 Validation of the Global Ocean Data Assimilation System (GODAS) data in the NOAA National Centre for Environmental System (NCEP) by theory, Comparative Studies, Applications and Sea Truth. IOTC-2011-WPB09-11.
41. Weaver, A. J. *et al.* The UVic Earth System Climate Model: Model description, climatology, and applications to past, present and future climates. *Atmos.-Ocean* **39,** 361–428 (2001).
42. Abraham, J. P. *et al.* A review of global ocean temperature observations: Implications for ocean heat content estimates and climate change. *Rev. Geophys.* **51,** 450–483 (2013).
43. Meinshausen, M. *et al.* The RCP greenhouse gas concentrations and their extension from 1765 to 2300. *Climatic Change* **109,** 213–241 (2011).
44. Phipps, S. J. *et al.* Paleoclimate data-model comparison and the role of climate forcings over the past 1500 years. *J. Clim.* **26,** 6915–6936 (2013).
45. Santoso, A., England, M. H. & Cai, W. Impact of Indo-Pacific feedback interactions on ENSO dynamics diagnosed using ensemble climate simulations. *J. Clim.* **25,** 7743–7763 (2012).
46. Meehl, G. A. *et al.* The WCRP CMIP3 multi-model dataset: A new era in climate change research. *Bull. Am. Meteorol. Soc.* **88,** 1383–1394 (2007).

Acknowledgements

Author contributions

M.H.E. conceived the study and wrote the initial draft of the paper. M.H.E., S.M. and P.S. formulated the experimental design and observational data analyses. P.S. conducted and analysed the ocean model experiments, S.M. analysed the observational data. M.H.E. designed and A.P. computed the analysis of the CMIP5 experiments, A.S.G. analysed the ocean reanalysis trends and A.S. ran the coupled model experiments. All authors contributed to interpreting the results, discussion of the associated dynamics and refinement of the paper.

Additional information

Supplementary information is available in the online version of the paper. Reprints and permissions information is available online at www.nature.com/reprints. Correspondence and requests for materials should be addressed to M.H.E.

Competing financial interests

The authors declare no competing financial interests.